Hindawi
Advances in High Energy Physics
Volume 2020, Article ID 6742578, 16 pages
https://doi.org/10.1155/2020/6742578

Research Article

A New Description of Transverse Momentum Spectra of Identified Particles Produced in Proton-Proton Collisions at High Energies

Pei-Pin Yang,[1,2] Fu-Hu Liu,[1,2] and Raghunath Sahoo[3]

[1] *Institute of Theoretical Physics & State Key Laboratory of Quantum Optics and Quantum Optics Devices, Shanxi University, Taiyuan, Shanxi 030006, China*
[2] *Collaborative Innovation Center of Extreme Optics, Shanxi University, Taiyuan, Shanxi 030006, China*
[3] *Discipline of Physics, School of Basic Sciences, Indian Institute of Technology Indore, Simrol, Indore 453552, India*

Correspondence should be addressed to Fu-Hu Liu; fuhuliu@163.com

Received 7 August 2020; Accepted 27 September 2020; Published 30 October 2020

Academic Editor: Enrico Lunghi

The transverse momentum spectra of identified particles produced in high energy proton-proton $(p+p)$ collisions are empirically described by a new method with the framework of the participant quark model or the multisource model at the quark level, in which the source itself is exactly the participant quark. Each participant (constituent) quark contributes to the transverse momentum spectrum, which is described by the TP-like function, a revised Tsallis–Pareto-type function. The transverse momentum spectrum of the hadron is the convolution of two or more TP-like functions. For a lepton, the transverse momentum spectrum is the convolution of two TP-like functions due to two participant quarks, e.g., projectile and target quarks, taking part in the collisions. A discussed theoretical approach seems to describe the $p+p$ collisions data at center-of-mass energy $\sqrt{s}=200$ GeV, 2.76 TeV, and 13 TeV very well.

1. Introduction

As one of the "first day" measurable quantities, the transverse momentum (p_{T}) spectra of various particles produced in high energy proton-proton $(p+p)$ (hadron-hadron), proton-nucleus (hadron-nucleus), and nucleus-nucleus collisions are of special importance because it reveals about the excitation degree and anisotropic collectivity in the produced systems. The distribution range of p_{T} is generally very wide, from 0 to more than 100 GeV/c, which is collision energy dependent. In the very low-, low-, high-, and very high-p_{T} regions [1], the shapes of p_{T} spectrum for given particles are possibly different from each other. In some cases, the differences are very large, and the spectra show different empirical laws.

Generally, the spectrum in (very) low-p_{T} region contributed by (resonance decays or other) soft excitation process. The spectrum in (very) high-p_{T} region is related to (very) hard scattering process (pQCD). There is no clear boundary in p_{T} to separate soft and hard processes. At a given collision energy, for different collision species, looking into the spectral shape, a theoretical function that best fits to the p_{T}-spectra is usually chosen to extract information like rapidity density, dN/dy, kinetic freeze-out temperature, T_{kin} or T_0 and average radial flow velocity, $\langle\beta_T\rangle$ orβ_T. The low-p_{T} region up to ~2–3 GeV/c is well described by a Boltzmann–Gibbs function, whereas the high-p_{T} part is dominated by a power-law tail. It is interesting to note that there are many different functions, sometimes motivated by the experimental trend of the data or sometimes theoretically, to have a proper spectral description thereby leading to a physical picture. The widely used functions are:

(1) An exponential function in p_{T} or m_{T} [2, 3]

$$\begin{aligned} f(p_{\mathrm{T}}) &= p_{\mathrm{T}} \times A \times \left(e^{-p_{\mathrm{T}}/T}\right) \times \frac{e^{m_0/T}}{T^2 + Tm_0}, \\ f(p_{\mathrm{T}}) &= p_{\mathrm{T}} \times A \times \left(e^{-m_{\mathrm{T}}/T}\right) \times \frac{e^{m_0/T}}{T^2 + Tm_0}. \end{aligned} \tag{1}$$

Here, A is the normalization constant, T is the effective temperature (thermal temperature and collective radial flow), and $m_\mathrm{T} = \sqrt{p_\mathrm{T}^2 + m_0^2}$ is the transverse mass, with m_0 being the identified particle rest mass.

(2) A Boltzmann distribution

$$f(p_\mathrm{T}) = p_\mathrm{T} \times A \times m_\mathrm{T} \times \left(e^{-m_\mathrm{T}/T}\right) \times \frac{e^{m_0/T}}{2T^3 + 2T^2 m_0 + T m_0^2}. \tag{2}$$

(3) Bose–Einstein/Fermi–Dirac distribution

$$f(p_\mathrm{T}) = p_\mathrm{T} \times A \times m_\mathrm{T} \times \frac{1}{e^{m_\mathrm{T}/T} \mp 1} \times \left(e^{m_0/T} \mp 1\right). \tag{3}$$

(4) Power-law or Hagedorn function [4]

$$f(p_\mathrm{T}) = p_\mathrm{T} \times A \times \left(1 + \frac{p_\mathrm{T}}{p_0}\right)^{-n} \longrightarrow \begin{cases} \exp\left(-\dfrac{n p_\mathrm{T}}{p_0}\right), & \text{for } p_\mathrm{T} \to 0, \\ \left(\dfrac{p_0}{p_\mathrm{T}}\right)^n, & \text{for } p_\mathrm{T} \to \infty, \end{cases} \tag{4}$$

where p_0 and n are fitting parameters. This becomes a purely exponential function for small p_T and a purely power-law function for large p_T values.

(5) Tsallis–Levy [5, 6] or Tsallis–Pareto-type function [6–9]

$$f(p_\mathrm{T}) = p_\mathrm{T} \times \frac{A(n-1)(n-2)}{nT[nT + m_0(n-2)]} \times \left(1 + \frac{m_\mathrm{T} - m_0}{nT}\right)^{-n}. \tag{5}$$

Note here that a multiplicative prefactor of p_T in the above functions are used assuming that the p_T spectra do not have a p_T factor in the denominator (see the expression for the invariant yield) and all the functions are normalized so that the integral of the functions provides the value of "A ." When the first three functions describe thep_T-spectra up to a low$p_\mathrm{T}$around 2–3 GeV/c, the fourth function, i.e., the power-law, describes the high$p_\mathrm{T}$part of the spectrum. The last two functions (power-law or Hagedorn function and Tsallis-L{\'e}vy or Tsallis–Pareto-type function), which are more empirical in nature, lack microscopic picture, however, describe a wide variety of identified particle spectra. The Tsallis distribution function, while describing the spectra in $p + p$ collisions [10], has brought up the concept of nonextensive entropy, contrary to the low-p_T domain pointing to an equilibrated system usually described by Boltzmann–Gibbs extensive entropy. In addition, the identified particle spectra are successfully explained in heavy ion collisions with the inclusion of radial flow in a Tsallis Blast Wave description [11].

The two behaviors in (very) low- and (very) high-p_T regions are difficult to fit simultaneously by a simple probability density function. Instead, one can use a two-component function [12], the first component $f_1(p_\mathrm{T})$ is for the (very) low-p_T region and the second component $f_2(p_\mathrm{T})$ is for the (very) high-p_T region, to superpose a new function $f(p_\mathrm{T})$ to fit the p_T spectra. There are two forms of superpositions, $f(p_\mathrm{T}) = kf_1(p_\mathrm{T}) + (1-k)f_2(p_\mathrm{T})$ or $f(p_\mathrm{T}) = A_1\theta(p_1 - p_\mathrm{T})f_1(p_\mathrm{T}) + A_2\theta(p_\mathrm{T} - p_1)f_2(p_\mathrm{T})$ [4, 13, 14], where k denotes the contribution fraction of the first component, A_1 and A_2 are constants which make the two components equal to each other at $p_\mathrm{T} = p_1$, and $\theta(x)$ is the usual step function which satisfies $\theta(x) = 0$ if $x < 0$ and $\theta(x) = 1$ if $x \geq 0$.

It is known that there are correlations in determining parameters in the two components in the first superposition [13]. There is possibly a nonsmooth interlinkage at $p_\mathrm{T} = p_1$ between the two components in the second superposition [14]. We do not expect these two issues. To avoid the correlations and nonsmooth interlinkage, we hope to use a new function to fit simultaneously the spectra in the whole p_T region for various particles. After sounding many functions out, a Tsallis–Pareto-type function [6–9] which empirically describes both the low-p_T exponential and the high-p_T power-law [15–18] is the closest to our target, though the Tsallis–Pareto-type function is needed to revise its form in some cases.

In this work, to describe the spectra in the whole p_T range which includes (very) low and (very) high p_T regions, the Tsallis–Pareto-type function is empirically revised by a simple method. To describe the spectra in the whole p_T range as accurately as possible, the contribution of participant quark to the spectrum is also empirically taken to be the revised Tsallis–Pareto-type (TP-like) function with another set of parameters. Then, the p_T distribution of given particles is a convolution of a few TP-like functions. To describe the spectra of identified particles in the whole p_T range, both the TP-like function and the convolution of a few TP-like functions are used to fit the data measured in $p + p$ collisions at the center-of-mass energy $\sqrt{s} = 200$ GeV [19–23], 2.76 TeV [24–32], and 13 TeV [33–39] by different collaborations.

The remainder of this paper is structured as follows. The formalism and method are described in Section 1. The results and discussion are given in Section 2. In Section 3, we summarize our main observations and conclusions.

2. Formalism and Method

According to [6–9], the Tsallis–Pareto-type function which empirically describes both the low-p_T exponential and the high-p_T power-law can be simplified as presented in [15–18],

$$f(p_\mathrm{T}) = C \times p_\mathrm{T} \times \left(1 + \frac{\sqrt{p_\mathrm{T}^2 + m_0^2} - m_0}{nT}\right)^{-n}, \tag{6}$$

in terms of p_{T} probability density function, where the parameter T describes the excitation degree of the considered source, the parameter n describes the degree of nonequilibrium of the considered source, and C is the normalization constant which depends on T, n, and m_0. Equation (6) is in fact an improvement of Eq. (5).

As an empirical formula, the Tsallis–Pareto-type function is successful in the description of p_{T} spectra in many cases. However, our exploratory analysis shows that Eq. (6) in some cases is not accurate in describing the spectra in the whole p_{T} range. In particular, Eq. (6) is not flexible enough to describe the spectra in a very low-p_{T} region, which is contributed by the resonance decays. We would like to revise empirically Eq. (6) by adding a power index a_0 on p_{T}. After the revision, we have

$$f(p_{\mathrm{T}}) = C \times p_{\mathrm{T}}^{a_0} \times \left(1 + \frac{\sqrt{p_{\mathrm{T}}^2 + m_0^2} - m_0}{nT}\right)^{-n}, \quad (7)$$

where C is the normalization constant which is different from that in Eq. (6). To be convenient, the two normalization constants in Eqs. (6) and (7) are denoted by the same symbol C. Equation (7) can be used to fit the spectra in the whole p_{T} range. The revised Tsallis–Pareto-type function (Eq. (7)) is called the TP-like function by us.

It should be noted that the index a_0 is a quantity with nondimension. Because of the introduction of a_0, the dimension of $p_{\mathrm{T}}^{a_0}$ is $(\mathrm{GeV/c})^{a_0}$. The dimension of $p_{\mathrm{T}}^{a_0}$ does not affect the dimension $(\mathrm{GeV}/c)^{-1}$ of $f(p_{\mathrm{T}})$. In fact, to fit the dimension of $f(p_{\mathrm{T}})$, the dimension of the product $Cp_{\mathrm{T}}^{a_0}$ is limited to be $(\mathrm{GeV}/c)^{-1}$. That is to say, the dimension of $p_{\mathrm{T}}^{a_0}$ is combined in the normalization constant so that we can obtain the consistent dimension for both sides of the equation. Due to the introduction of a_0, for the spectra in the very low-p_{T} region, not only the production of light particles via resonance decay but also the decay or absorbtion effect of heavy particles in the hot and dense medium in the participant region can be described.

Our exploratory analysis shows that Eq. (7) is not accurate in describing the spectra in the whole p_{T} range, too, though it is more accurate than Eq. (6). To obtain accurate results, the amount or portion (p_{ti}) contributed by the ith participant quark to p_{T} is assumed to obey

$$f_i(p_{ti}) = C_i \times p_{ti}^{a_0} \times \left(1 + \frac{\sqrt{p_{ti}^2 + m_{0i}^2} - m_{0i}}{nT}\right)^{-n}, \quad (8)$$

where the subscript i is used for the quantities related to the participant quark i, and m_{0i} is empirically the constituent mass of the considered quark i. The value of i can be 2 or 3 even 4 or 5 due to the number of participant (or constituent) quarks. Equation Eq. (8) is also the TP-like function with different mass from Eq. (7).

It should be noted that m_0 in Eq. (7) is for a particle and m_{0i} in Eq. (8) is for the quark i. For example, if we study the p_{T} spectrum of protons, we have $m_0 = 0.938\,\mathrm{GeV}/c^2$ and $m_{01} = m_{02} = m_{03} = 0.31\,\mathrm{GeV}/c^2$. In the case of studying the p_{T} spectrum of photons, we have $m_0 = 0$ and $m_{01} = m_{02} = 0.31\,\mathrm{GeV}/c^2$ if we assume that the two lightest quarks take part in the collision with photon production.

There are two participant quarks to constitute usually mesons, namely the quarks 1 and 2. The p_{T} spectra of mesons are the convolution of two TP-like functions.

We have

$$f(p_{\mathrm{T}}) = \int_0^{p_{\mathrm{T}}} f_1(p_{t1}) f_2(p_{\mathrm{T}} - p_{t1})\, dp_{t1} = \int_0^{p_{\mathrm{T}}} f_2(p_{t2}) f_1(p_{\mathrm{T}} - p_{t2})\, dp_{t2}, \quad (9)$$

in which $f_1(p_{t1})\, f_2(p_{t2})$ is the probability for the given p_{t1} and p_{t2}. The total probability considered various p_{t1} and p_{t2} is given by Eq. (9) which is the convolution of distributions of two independent variables [40, 41]. The upper limit p_T is not a cutoff, but the sum of p_{t1} and p_{t2}, which is limited by physics. The lower limit 0 is also from the limitation related to the underlying physics. No matter how many leptons are produced in the process, two participant quarks are considered to contribute to the p_T spectrum of each lepton.

We would like to explain our treatment on Eq. (9) here. At least three relations between particle p_{T} and quark p_{t1} (p_{t2}) can be assumed. (i) If we regard p_{t1} (p_{t2}) as the amount or portion contributed by the first (second) participant quark to p_{T}, we have $p_{\mathrm{T}} = p_{t1} + p_{t2}$. (ii) If we regard the vector p_{t1}(p_{t2}) as the component contributed by the first (second) participant quark to the vector p_{T}, we have $p_{\mathrm{T}} = \sqrt{p_{t1}^2 + p_{t2}^2}$, where p_{t1} is perpendicular to p_{t2}. (iii) In the second relation, it is not necessary that all the components are perpendicular, then we have $p_{\mathrm{T}} = \sqrt{p_{t1}^2 + p_{t2}^2 + 2p_{t1}p_{t2}\cos|\phi_1 - \phi_2|}$, where $\phi_1(\phi_2)$ is the azimuthal angle of the first (second) participant quark. Different assumptions result in different relations. Of course, the three p_{t1} (p_{t2}) in the three relations have different meanings, though the same symbol is used. In our opinion, at present, it is hard to say which relation is more correct. We need to test the three relations by more experimental data.

In fact, all the three relations have still pending issues which needed further discussions. In the relation (i), although p_{T} can be considered as the contribution of two energy sources: the first and second participant quarks that contribute the amounts or portions p_{t1} and p_{p2} to p_T, respectively, the vector characteristic of transverse momentum is not used. In the relation (ii), as a vector, the transverse momentum is considered by two components: p_{t1} and p_{t2} which are contributed by the first and second participant quarks, respectively, though the origin of the third component of meson momentum is not clear. In addition, although the origin of three components of baryon momentum is clear, the physics picture is not consistent to the meson momentum. In the relation (iii), two more parameters ϕ_1 and ϕ_2 are introduced, which is not our expectation.

This paper has used the relation (i) and Eq. (9) which is based on the probability theory [40–42]. However, in our recent work [43], we have used the relation (ii) and another functional form which is based on the vector and probability theory [41, 42]. We hope that we may use the relation (iii) in our future work by some limitations on ϕ_1 and ϕ_2. The relation (i) in terms of amount or portion is the same as or similar to the relation for multiplicity or transverse energy contributed by two sources [40]. This similarity reflects the law of universality existing in high energy collisions [44–49]. In fact, transverse momentum, multiplicity, and transverse energy reflect the amount of effective energy deposited in collisions [50, 51]. The effective energy through the participant quarks reflects the similarity or universality, which is not related to the production mechanisms for different particles. Then, different particles are described by the same type of model (formula).

At the level of current knowledge, leptons have no further structures. However, to produce a lepton in a common process, two participant quarks, a projectile quark and a target quark, are assumed to take part in the interactions. The p_{T} spectra of leptons are in fact the convolution of two TP-like functions, that is Eq. (9) in which m_{01} and m_{02} are empirically the constituent mass of the lightest quark. To produce leptons in a special process such as in $c\bar{c} \to \mu^+\mu^-$, m_{01} (m_{02}) is the constituent mass of the c quark.

There are three participant quarks that constitute usually baryons, namely the quarks 1, 2, and 3. The p_{T} spectra of baryons are the convolution of three TP-like functions. We have the convolution of the first two TP-like functions to be

$$f_{12}(p_{t12}) = \int_0^{p_{t12}} f_1(p_{t1}) f_2(p_{t12} - p_{t1}) dp_{t1} = \int_0^{p_{t12}} f_2(p_{t2}) f_1(p_{t12} - p_{t2}) dp_{t2}. \tag{10}$$

The convolution of the first two TP-like functions and the third TP-like function is

$$f(p_{\mathrm{T}}) = \int_0^{p_{\mathrm{T}}} f_{12}(p_{t12}) f_3(p_{\mathrm{T}} - p_{t12}) dp_{t12} = \int_0^{p_{\mathrm{T}}} f_3(p_{t3}) f_{12}(p_{\mathrm{T}} - p_{t3}) dp_{t3}. \tag{11}$$

Equation (7) can fit approximately the spectra in the whole p_{T} range for various particles at the particle level, in which m_0 is the rest mass of the considered particle. In principle, Eqs. (9) and (11) can fit the spectra in the whole p_{T} range for various particles at the quark level, in which m_{0i} is the constituent mass of the quark i. If Eq. (7) is more suitable than Eq. (6), Eqs. (9) and (11) are the results of the multisource model [52, 53] at the quark level. In the multisource model, one, two, or more sources are assumed to emit particles due to different production mechanisms, source temperatures, and event samples. In a given event sample, the particles with the same source temperature are assumed to emit from the same source by the same production mechanism. We can also call Eqs. (9) and (11) the results of the participant quark model due to the fact that they describe the contributions of participant quarks.

It should be noted that, in principle, the three quarks should be symmetric in the formula for the production of baryons. Indeed, in Eqs. (10) and (11), the two momenta $p_{t,1}$ and $p_{t,2}$ are symmetric, and the third momentum $p_{t,3}$ is also symmetric to the other two momenta. In fact, according to the rule of the convolution of three functions, we may also convolute firstly the last two functions, and then, we may convolute the result with the first function. Meanwhile, we may also convolute firstly the first and third functions, and then, we may convolute the result with the second function. We realize that the final result is not related to the order of convolution. The three functions contributed by the three quarks are indeed symmetric.

We would like to explain the normalization constant in detail. As a probability density function, $f(p_{\mathrm{T}}) = (1/N)dN/dp_{\mathrm{T}}$ cannot be used to compare directly with the experimental data presented in the literature in some cases, where N denotes the number of considered particles. Generally, the experimental data are presented in forms of (i) dN/dp_{T}, (ii) $d^2N/dydp_{\mathrm{T}}$, and (iii) $(1/2\pi p_{\mathrm{T}})d^2N/dydp_{\mathrm{T}} = Ed^3N/dp^3$, where E (p) denotes the energy (momentum) of the considered particle. One can use $N_0 f(p_{\mathrm{T}})$, $N_0 f(p_{\mathrm{T}})/dy$, and $(1/2\pi p_{\mathrm{T}})N_0 f(p_{\mathrm{T}})/dy$ to fit them accordingly, where N_0 denotes the normalization constant.

The data are usually in the form (i) $d\sigma/dp_{\mathrm{T}}$, (ii) $d^2\sigma/dydp_{\mathrm{T}}$, and (iii) $(1/2\pi p_{\mathrm{T}})d^2\sigma/dydp_{\mathrm{T}} = Ed^3\sigma/dp^3$, where σ denotes the cross-section. One can use $\sigma_0 f(p_{\mathrm{T}})$, $\sigma_0 f(p_{\mathrm{T}})/dy$, and $(1/2\pi p_{\mathrm{T}})\sigma_0 f(p_{\mathrm{T}})/dy$ to fit them accordingly, where σ_0 denotes the normalization constant. The data presented in terms of m_{T} can also be studied due to the conserved probability density and the relation between m_{T} and p_{T}. In particular, $(1/2\pi p_{\mathrm{T}})d^2\sigma/dydp_{\mathrm{T}} = (1/2\pi m_{\mathrm{T}})d^2\sigma/dydm_{\mathrm{T}}$, where σ can be replaced by N.

It should be noted that our treatment procedure means that the parameters are fitted for each energy and rapidity bin separately. This would limit the usefulness of the proposed parametrizations somewhat. However, after obtaining the relations between parameters and energy/rapidity, we can use the obtained fits to predict p_{T} distributions at other energies/rapidities where the data are not available and the parameters are not fitted.

3. Results and Discussion

3.1. Comparison with Data. Figure 1(a) shows the p_{T} spectra (the invariant cross-sections), $Ed^3\sigma/dp^3$, of different hadrons with given combinations and decay channels including $(\pi^+ + \pi^-)/2$ plus $\pi^0 \to \gamma\gamma$, $(K^+ + K^-)/2$ plus $K_S^0 \to \pi^0\pi^0$, $\eta \to \gamma\gamma$ plus $\eta \to \pi^0\pi^+\pi^-$; $\omega \to e^+e^-$ plus $\omega \to \pi^0\pi^+\pi^-$ plus $\omega \to \pi^0\gamma$, $(p + \bar{p})/2$, $\eta' \to \eta\pi^+\pi^-$, $\phi \to e^+e^-$ plus $\phi \to K^+K^-$, $J/\psi \to e^+e^-$, and $\psi' \to e^+e^-$ produced in $p + p$ collisions at 200 GeV. Different symbols represent different particles and their different decay channels measured by the PHENIX Collaboration [19] in the pseudorapidity range of $|\eta| < 0.35$. The results corresponding to π, K, η, ω, p, and η' are rescaled by multiplying by 10^6, 10^5, 10^4, 10^3, 10^2, and 10 factors, respectively. The results corresponding to ϕ, J/ψ, and ψ' are not rescaled.

In Figure 1(a), the dotted and dashed curves are our fitted results by using Eqs. (7) (for mesons and baryons) and (9) (for mesons) or (11) (for baryons), respectively. The values

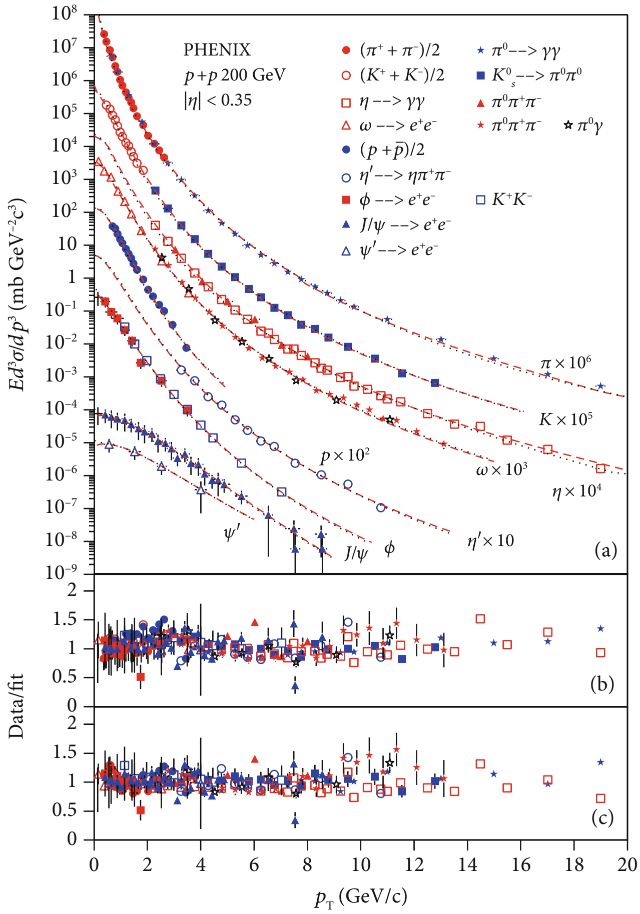

Figure 1: (a) The invariant cross-sections of different hadrons with given combinations and decay channels produced in $p+p$ collisions at 200 GeV. Different symbols represent different particles and their different decay channels in $|\eta| < 0.35$ measured by the PHENIX Collaboration [19]; some of them are scaled by different factors marked in the panel. The dotted and dashed curves are our fitted results by using Eqs. (7) and (9) or (11), respectively. (b) The ratio of data to fit obtained from Eq. (7). (c) The ratio of data to fit obtained from Eq. (9) or (11).

of free parameters (T, n, and a_0), normalization constant (σ_0), χ^2, and the number of degree of freedom (ndof) obtained from Eq. (7) are listed in Table 1, while the values of parameters and χ^2/ndof obtained from Eqs. (9) or (11) are listed in Table 2. In Eq. (7), m_0 is taken to be the rest mass of π, K, η, ω, p, η', ϕ, J/ψ, and ψ' for the cases from $(\pi^+ + \pi^-)/2$ to $\psi' \to e^+e^-$ sequenced according to the order shown in Figure 1(a). In the fit process at the quark level, the quark structure of π^0 results in its $f(p_T)$ to be the half of the sum of $u\bar{u}$'s $f(p_T)$ and $d\bar{d}$'s $f(p_T)$. Because the constituent masses of u and d are the same [54], π^0's $f(p_T)$ is equal to $u\bar{u}$'s $f(p_T)$ or $d\bar{d}$'s $f(p_T)$. The quark structure of η results in its $f(p_T)$ to be $\cos^2\phi \times u\bar{u}$'s $f(p_T) + \sin^2\phi \times s\bar{s}$'s $f(p_T)$ due to the quark structures of η_q and η_s, where $\phi = 39.3^\circ \pm 1.0^\circ$ is the mixing angle [55]. The quark structure of η' results in its $f(p_T)$ to be $\sin^2\phi \times u\bar{u}$'s $f(p_T) + \cos^2\phi \times s\bar{s}$'s $f(p_T)$.

To show departures of the fit from the data, following Figure 1(a), Figures 1(b) and 1(c) show the ratios of data to fit obtained from Eqs. (7) and (9) or (11), respectively. One can see that the fits are around the data in the whole p_T range, except for a few sizeable departures. The experimental data for the mentioned hadrons measured in $p+p$ collisions at 200 GeV by the PHENIX Collaboration [19] can be fitted by Eqs. (7) (for mesons and baryons) and (9) (for mesons) or (11) (for baryons). From the values of χ^2 and the data over fit ratio, one can see that Eq. (9) or (11) can describe the data equally well as Eq. (7).

It seems that Eq. (9) or (11) is not necessary due to Eq. (7) being good enough. In fact, the introduction of Eq. (9) or (11) does not contain more parameters compared with Eq. (7). Moreover, Eq. (9) or (11) can tell more about the underlying physics than Eq. (7). The effective temperature used in Eq. (9) or (11) is related to the excitation degree of quark matter, while the effective temperature in Eq. (7) is related to the excitation degree of hadronic matter. In our opinion, Eqs. (9) and (11) are necessary. We shall analyze sequentially the p_T spectra of identified particles by using Eqs. (7) and (9) or (11) in the following text.

Figure 2(a) shows the invariant cross-sections of inclusive direct photons and different leptons with given combinations and production channels including $(e^+ + e^-)/2$, $(\mu^+ + \mu^-)/2$ (open heavy-flavor decays), Drell–Yan $\to \mu^+\mu^-$, $c\bar{c} \to \mu^+\mu^-$, and $b\bar{b} \to \mu^\pm\mu^\pm$ produced in $p+p$ collisions at 200 GeV. Different symbols represent different particles and their production channels measured by the PHENIX Collaboration [20–23] in different η or y ranges. The dotted and dashed curves are our fitted results by using Eqs. (7) and (9), respectively, where two participant quarks are considered in the formation of the mentioned particles. The values of parameters and χ^2/ndof obtained from Eqs. (7) and (9) are listed in Tables 3 and 4, respectively. In Eq. (7), m_0 is taken to be the rest mass of γ, e, μ, 2μ, 2μ, and 4μ for the cases from inclusive direct γ to $b\bar{b} \to \mu^\pm\mu^\pm$ sequenced according to the order shown in Figure 2(a), where 2μ is two times due to the continued two 2μ-related channels. In Eq. (9), $m_{01} + m_{02}$ are taken to be the constituent masses of $u+u$, $u+u$, $u+c$, $u+u$, $c+c$, and $b+b$ sequenced according to the same order as particles.

Following Figure 2(a), Figures 2(b) and 2(c) show the ratios of data to fit obtained from Eqs. (7) and (9), respectively. One can see that the fits of the data are rather good in the whole p_T range, except for a few sizeable departures. The experimental data on the mentioned photons and leptons measured in $p+p$ collisions at 200 GeV by the PHENIX Collaboration [20–23] can also be fitted by Eqs. (7) and (9). From the values of χ^2 and the data over fit ratio, one can see that Eq. (9) can describe the data equally well as Eq. (7).

Similar to Figure 1(a), Figure 3(a) show the invariant cross-sections of various hadrons produced in $p+p$ collisions at 2.76 TeV. Different symbols represent different particles measured by the ALICE Collaboration [24–28] in different η or y ranges. The values of parameters and χ^2/ndof are listed in Table 1. The fit of ρ at the quark level is the same with π^0. Other particles and corresponding quarks are discussed in

Table 1: Values of T, n, a_0, σ_0, χ^2, and ndof corresponding to the dotted curves in Figures 1(a), 3(a), and 5(a) which are fitted by the TP-like function (Eq. (7)). In the case of ndof being less than 1, it appears as "–" in the table.

Figure	$y(\eta)$	Particle	T (GeV)	n	a_0	σ_0 (mb)	χ^2/ndof
Figure 1(a) 200 GeV	$\|\eta\| < 0.35$	$(\pi^+ + \pi^-)/2$ π^0	0.129 ± 0.001	9.449 ± 0.020	0.890 ± 0.004	37.044 ± 0.348	5/39
		$(\mathrm{K}^+ + \mathrm{K}^-)/2$ K_S^0	0.167 ± 0.002	9.529 ± 0.030	1.027 ± 0.004	3.122 ± 0.030	7/27
		η	0.195 ± 0.002	9.889 ± 0.033	1.000 ± 0.003	1.755 ± 0.087	6/32
		ω	0.193 ± 0.001	9.460 ± 0.100	0.900 ± 0.020	3.073 ± 0.030	23/34
		$(p + \bar{p})/2$	0.149 ± 0.002	9.100 ± 0.020	1.040 ± 0.003	1.291 ± 0.008	11/13
		η'	0.210 ± 0.002	10.001 ± 0.023	0.980 ± 0.003	0.584 ± 0.004	4/8
		ϕ	0.245 ± 0.002	10.559 ± 0.023	0.688 ± 0.003	0.334 ± 0.003	10/15
		J/ψ	0.482 ± 0.002	16.778 ± 0.023	0.901 ± 0.004	$(5.320 \pm 0.132) \times 10^{-4}$	4/22
		ψ'	0.452 ± 0.002	8.349 ± 0.022	0.959 ± 0.003	$(9.234 \pm 0.008) \times 10^{-5}$	1/–
Figure 3(a) 2.76 TeV	$\|\eta\| < 0\ .8$	$\pi^+ + \pi^-$	0.130 ± 0.001	6.882 ± 0.021	0.937 ± 0.002	$(3.961 \pm 0.032) \times 10^2$	46/59
		$K^+ + K^-$	0.167 ± 0.001	6.985 ± 0.019	1.209 ± 0.003	47.404 ± 0.649	32/54
		$p + \bar{p}$	0.199 ± 0.001	7.870 ± 0.024	1.064 ± 0.003	23.645 ± 0.129	56/45
	$\|y\| < 0\ .\ 5$	$\rho^0(770)$	0.205 ± 0.001	6.987 ± 0.021	1.140 ± 0.003	14.167 ± 0.069	6/6
		ϕ	0.245 ± 0.002	6.696 ± 0.021	1.010 ± 0.004	1.673 ± 0.016	7/17
	$\|y\| < 0\ .\ 8$	η	0.195 ± 0.001	6.910 ± 0.024	1.023 ± 0.003	$(3.340 \pm 0.064) \times 10^{-10}$	7/7
	$2\ .\ 5 < y < 4$	J/ψ	0.482 ± 0.002	7.231 ± 0.025	1.225 ± 0.003	$(2.181 \pm 0.029) \times 10^{-2}$	4/3
Figure 5(a) 13 TeV	$\|y\| < 1$	$(\pi^+ + \pi^-)/2$	0.129 ± 0.001	4.862 ± 0.021	0.806 ± 0.003	$(4.608 \pm 0.018) \times 10^2$	57/18
		$(K^+ + K^-)/2$	0.167 ± 0.001	6.179 ± 0.018	1.261 ± 0.002	$(4.312 \pm 0.039) \times 10^1$	3/13
		$(p + \bar{p})/2$	0.199 ± 0.002	4.768 ± 0.023	1.180 ± 0.004	$(2.211 \pm 0.013) \times 10^1$	8/22
	$2 < y < 2.5$	J/ψ prompt	0.482 ± 0.001	6.729 ± 0.022	1.581 ± 0.003	$(1.097 \pm 0.001) \times 10^{-2}$	115/10
		J/ψ from b	0.482 ± 0.001	5.529 ± 0.024	1.877 ± 0.002	$(1.850 \pm 0.020) \times 10^{-3}$	35/10
		$\psi(2s)$ prompt	0.578 ± 0.001	7.603 ± 0.021	1.867 ± 0.003	$(1.509 \pm 0.019) \times 10^{-3}$	33/13
		$\psi(2s)$ from b	0.578 ± 0.001	5.989 ± 0.023	1.901 ± 0.004	$(4.907 \pm 0.104) \times 10^{-4}$	33/13
		$\mathrm{D}^0 + \bar{\mathrm{D}}^0$	0.497 ± 0.001	6.624 ± 0.022	1.244 ± 0.003	$(5.573 \pm 0.063) \times 10^{-1}$	5/14
		$\mathrm{D}^+ + \mathrm{D}^-$	0.497 ± 0.002	6.446 ± 0.022	1.231 ± 0.005	$(2.805 \pm 0.059) \times 10^{-1}$	11/13
		$\mathrm{D}^{*+} + \mathrm{D}^{*-}$	0.497 ± 0.001	6.566 ± 0.023	1.231 ± 0.004	$(2.622 \pm 0.054) \times 10^{-1}$	16/11
		$\mathrm{D}_s^+ + \mathrm{D}_s^-$	0.497 ± 0.001	9.259 ± 0.021	2.217 ± 0.004	$(7.876 \pm 0.149) \times 0^{-2}$	5/12

Figure 1(a). Similarly, Figures 3(b) and 3(c) show the ratios of data to fit obtained from Eqs. (7) and (9) or (11), respectively. One can see that the fits of the data are rather good in the whole p_T range, except for a few sizeable departures. The experimental data on the mentioned hadrons measured in $p + p$ collisions at 2.76 TeV by the ALICE Collaboration [24–28] can be fitted by Eqs. (7) and (9) or (11). From the values of χ^2 and the data over fit ratio, one can see that Eq. (9) or (11) can describe the data equally well as Eq. (7).

Similar to Figure 2(a), Figure 4(a) shows the invariant cross-sections of photons and different leptons with given combinations and production channels including inclusive γ, μ from heavy-flavor hadron decays, e from beauty hadron decays, e from heavy-flavor hadron decays, and inclusive ($e^+ + e^-$)/2 produced in $p + p$ collisions at 2.76 TeV. Different symbols represent different particles measured by the ALICE Collaboration [29–32] in different y ranges. The values of parameters and χ^2/ndof are listed in Table 2. In Eq. (7), m_0 is taken to be the rest mass of γ, μ, e, e, and e for the cases from inclusive γ to inclusive $(e^+ + e^-)/2$ sequenced according to the order shown in Figure 4(a), where e is three times due to the continued three e-related channels. In Eq. (9), $m_{01} + m_{02}$ are taken to be the constituent masses of $u + u$, $c + c$, $b + b$, $c + c$, and $u + u$ sequenced according to the same order as particles. Following Figures 4(a)–4(c) show the ratios of data to fit obtained from Eqs. (7) and (9), respectively. One

Table 2: Values of T, n, a_0, σ_0, χ^2, and ndof corresponding to the dashed curves in Figures 1(a), 3(a), and 5(a) which are fitted by the convolution (Eq. (9) or (11)) of two or three TP-like functions. The quark structures are listed together. In the case of ndof being less than 1, it appears as "–" in the table.

Figure	$y(\eta)$	Particle	Quark structure	T (GeV)	n	a_0	σ_0 (mb)	χ^2/ndof
Figure 1(a) 200 GeV	$\lvert\eta\rvert < 0.35$	$(\pi^+ + \pi^-)/2$	$u\bar{d}, d\bar{u}$	0.209 ± 0.002	7.774 ± 0.025	-0.540 ± 0.020	38.357 ± 0.350	6/39
		π^0	$(u\bar{u} - d\bar{d})/\sqrt{2}$					
		$(K^+ + K^-)/2$	$u\bar{s}, s\bar{u}$	0.196 ± 0.001	7.816 ± 0.030	-0.091 ± 0.005	2.913 ± 0.026	4/27
		K_S^0	$d\bar{s}$					
		$\eta : \eta_q, \eta_s$	$(u\bar{u} + d\bar{d})/\sqrt{2}, s\bar{s}$	0.212 ± 0.001	8.109 ± 0.030	0.000 ± 0.004	1.838 ± 0.017	4/32
		ω	$(u\bar{u} + d\bar{d})/\sqrt{2}$	0.222 ± 0.001	8.394 ± 0.013	0.000 ± 0.002	2.854 ± 0.026	20/34
		$(p + \bar{p})/2$	$uud, \bar{u}\bar{u}\bar{d}$	0.162 ± 0.002	7.600 ± 0.021	-0.130 ± 0.003	1.282 ± 0.011	3/13
		$\eta' : \eta_q, \eta_s$	$(u\bar{u} + d\bar{d})/\sqrt{2}, s\bar{s}$	0.233 ± 0.002	8.315 ± 0.025	0.000 ± 0.003	0.593 ± 0.004	3/8
		ϕ	$s\bar{s}$	0.266 ± 0.001	9.022 ± 0.022	-0.107 ± 0.003	0.319 ± 0.003	10/15
		J/ψ	$c\bar{c}$	0.509 ± 0.002	14.545 ± 0.025	0.008 ± 0.003	$(5.275 \pm 0.004) \times 10^{-4}$	4/22
		ψ'	$c\bar{c}$	0.503 ± 0.002	7.025 ± 0.030	0.055 ± 0.004	$(9.232 \pm 0.008) \times 10^{-5}$	1/–
Figure 3(a) 2.76 TeV	$\lvert\eta\rvert < 0.8$	$\pi^+ + \pi^-$	$u\bar{d}, d\bar{u}$	0.209 ± 0.001	4.970 ± 0.022	-0.490 ± 0.003	$(4.474 \pm 0.021) \times 10^2$	67/59
		$K^+ + K^-$	$u\bar{s}, s\bar{u}$	0.197 ± 0.002	5.223 ± 0.017	-0.058 ± 0.004	44.823 ± 0.605	30/54
		$p + \bar{p}$	$uud, \bar{u}\bar{u}\bar{d}$	0.194 ± 0.002	5.867 ± 0.021	-0.120 ± 0.003	24.401 ± 0.113	31/45
	$\lvert y\rvert < 0.5$	$\rho^0(770)$	$(u\bar{u} + d\bar{d})/\sqrt{2}$	0.252 ± 0.001	5.775 ± 0.021	-0.003 ± 0.003	14.514 ± 0.075	4/6
		ϕ	$s\bar{s}$	0.266 ± 0.001	5.313 ± 0.019	0.018 ± 0.001	1.679 ± 0.045	6/17
	$\lvert y\rvert < 0.8$	$\eta : \eta_q, \eta_s$	$(u\bar{u} + d\bar{d})/\sqrt{2}$	0.212 ± 0.002	5.341 ± 0.022	-0.021 ± 0.003	$(3.441 \pm 0.021) \times 10^{-10}$	10/7
	$2.5 < y < 4$	J/ψ	$c\bar{c}$	0.509 ± 0.002	6.181 ± 0.018	0.155 ± 0.004	$(2.179§0.007) \times 10^2$	4/3
Figure 5(a) 13 TeV	$\lvert y\rvert < 1$	$(\pi^+ + \pi^-)/2$	$u\bar{d}, d\bar{u}$	0.182 ± 0.001	4.401 ± 0.024	-0.390 ± 0.002	$(4.579 \pm 0.016) \times 10^2$	54/18
		$(K^+ + K^-)/2$	$u\bar{s}, s\bar{u}$	0.196 ± 0.001	7.081 ± 0.023	-0.023 ± 0.002	$(4.384 \times 0.016) \times 10^1$	1/13
		$(p + \bar{p})/2$	$uud, \bar{u}\bar{u}\bar{d}$	0.191 ± 0.001	3.832 ± 0.021	-0.090 ± 0.003	$(2.207 \pm 0.011) \times 10^1$	8/22
	$2 < y < 2.5$	J/ψ prompt	$c\bar{c}$	0.509 ± 0.001	4.855 ± 0.022	0.291 ± 0.003	$(1.056 \pm 0.002) \times 10^{-2}$	97/10
		J/ψ from b	$c\bar{c}$	0.509 ± 0.001	3.904 ± 0.023	0.447 ± 0.002	$(1.812 \pm 0.016) \times 10^{-3}$	28/10
		$\psi(2s)$ prompt	$c\bar{c}$	0.675 ± 0.002	6.098 ± 0.022	0.435 ± 0.003	$(1.490 \pm 0.017) \times 10^{-3}$	21/13
		$\psi(2s)$ from b	$c\bar{c}$	0.675 ± 0.002	4.531 ± 0.019	0.431 ± 0.004	$(4.836 \pm 0.059) \times 10^{-4}$	20/13
		$D^0 + \bar{D}^0$	$c\bar{u}, \bar{c}u$	0.545 ± 0.001	5.125 ± 0.017	0.104 ± 0.003	$(5.420 \pm 0.045) \times 10^{-1}$	3/14
		$D^+ + D^-$	$c\bar{d}, \bar{c}d$	0.545 ± 0.002	4.929 ± 0.023	0.098 ± 0.004	$(2.718 \times 0.043) \times 10^{-1}$	8/13
								14/11

Table 2: Continued.

Figure	y(η)	Particle	Quark structure	T (GeV)	n	a_0	σ_0 (mb)	χ^2/ndof
		$D^{*+} + D^{*-}$	$c\bar{d}, \bar{c}d$	0.545 ± 0.001	5.025 ± 0.019	0.101 ± 0.002	$(2.477 \pm 0.034) \times 10^{-1}$	
		$D_s^+ + D_s^-$	$c\bar{s}, \bar{c}s$	0.545 ± 0.001	6.515 ± 0.020	0.549 ± 0.003	$(7.406 \pm 0.099) \times 10^{-2}$	5/12

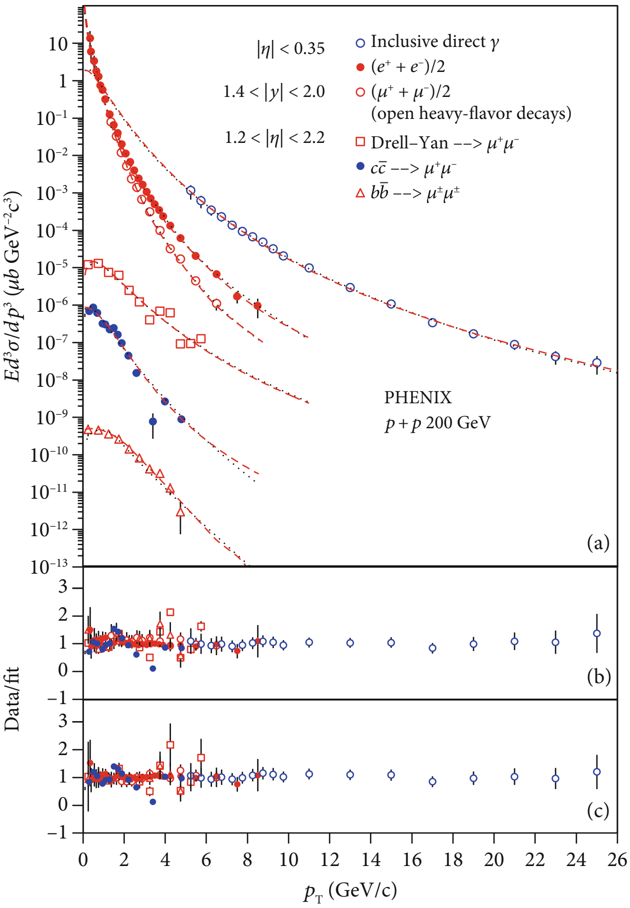

Figure 2: (a) The invariant cross-sections of photons and different leptons for a given combination of intermediate channel for $p + p$ collisions at 200 GeV. Different symbols represent different particles, and their production channels in different η ranges measured by the PHENIX Collaboration [20–23]. The dotted and dashed curves are our fitted results by using Eqs. (7) and (9), respectively. (b) The ratio of data to fit obtained from Eq. (7). (c) The ratio of data to fit obtained from Eq. (9).

can see that the fits agree with the data in the whole p_T range, except for a few departures. The experimental data on the mentioned photons and leptons measured in $p + p$ collisions at 2.76 TeV by the ALICE Collaboration [29–32] can be fitted by Eqs. (8) and (10). From the values of χ^2 and the data over fit ratio, one can see that Eq. (9) can describe the data equally well as Eq. (7).

Similar to Figures 1(a) and 3(a), Figure 5(a) shows the invariant cross-sections of different hadrons produced in $p + p$ collisions at 13 TeV. Different symbols represent different particles measured by the CMS [33] or LHCb [34–36] Collaborations in different y ranges. The values of parameters and χ^2/ndof are listed in Table 1. Except for the first five groups of particles and corresponding quarks which are discussed in Figure 1(a), m_0 in Eq. (7) for other particles is taken to be the rest mass of $\psi(2s)$, $\psi(2s)$, D^0, D^+, D^{*+}, and D_s^+ for the cases from $\psi(2s)$ prompt to $D_s^+ + D_s^-$ sequenced according to the order shown in Figure 5(a) from the left to right panels. Meanwhile, $m_{01} + m_{02}$ in Eq. (9) for other cases are taken to be the constituent masses of $c + c$, $c + c$, $c + u$, $c + d$, $c + d$, and $c + s$ sequenced according to the same order as particles. Following Figures 5(a)–5(c) show the ratio of data to fit obtained from Eqs. (7) and (9) or (11), respectively. One can see that the fits are close to the data in the whole p_T range, except for a few departures. The experimental data on the mentioned hadrons measured in $p + p$ collisions at 13 TeV by the CMS [33] and LHCb [34–36] Collaborations can be fitted by Eqs. (7) and (9) or (11). From the values of χ^2 and the data over fit ratio, one can see that Eq. (9) or (11) can describe the data equally well as Eq. (7).

Similar to Figures 2(a) and 4(a), Figure 6(a) shows the invariant cross-sections of $H \rightarrow$ diphotons and heavy flavor dielectrons produced in $p + p$ collisions at 13 TeV. Different symbols represent different particles measured by the ATLAS [37] or ALICE [38] Collaborations in different η ranges. The values of parameters and χ^2/ndof are listed in Table 2. In Eq. (7), m_0 is taken to be the rest masses of $2\gamma\,(=0)$ and $2e$ sequenced according to the order shown in Figure 6(a). In Eq. (9), both types of particles correspond to the same $m_{01} + m_{02}$, i.e., the constituent masses of $c + c$. Following Figures 6(a)–6(c) shows the ratios of data to fit obtained from Eqs. (7) and (9), respectively. One can see that the fits agree with the data in the whole p_T range, except for a few departures. The experimental data of diphotons and dielectrons measured in $p + p$ collisions at 13 TeV by the ATLAS [37] and ALICE [38] Collaborations can be fitted by Eqs. (8) and (10). From the values of χ^2 and the data over fit ratio, one can see that Eq. (9) can describe the data equally well as Eq. (7).

3.2. Discussion on Parameters. We now analyze the tendencies of the free parameters. The values of effective temperature T for the emissions of different hadrons do not depend on collision energy. This situation is different for the emissions of photons and leptons, in which there is a clear dependence on energy. This reflects that the emission processes of photons and leptons are more complex than those of hadrons. In the central (pseudo) rapidity region, T shows an incremental tendency with the increase of particle or quark mass. This is understandable that more collision energies are deposited to produce massive hadrons or to drive massive quarks to take part in the process of photon and lepton production. In the forward/backward (pseudo) rapidity region, T is expected to be less than that in the central (pseudo) rapidity region due to less energy deposited.

The values of power index n are very large with small fluctuations in this study. In the Tsallis statistics [6–9, 15–18], $n = 1/(q - 1)$, where q is an entropy index that characterizes the degree of equilibrium or nonequilibrium. Generally, $q = 1$ corresponds to an equilibrium state. A larger q than 1 corresponds to a nonequilibrium state. This study renders that the values of q are very close to 1, which means that the collision system considered by us is approximately in an equilibrium state. The functions based on statistical methods are applicable in this study. In particular, with the increasing collision energy, n decreases and then q increases slightly.

Table 3: Values of T, n, a_0, σ_0, χ^2, and ndof corresponding to the dotted curves in Figures 2(a), 4(a), and 6(a) which are fitted by the TP-like function (Eq. (7)).

Figure	$y(\eta)$	Particle	T (GeV)	n	a_0	σ_0 (mb)	χ^2/ndof
Figure 2(a) 200 GeV	$\lvert\eta\rvert < 0.35$	Inclusive direct γ	0.258 ± 0.001	9.413 ± 0.020	1.750 ± 0.004	$(4.836 \pm 0.044) \times 10^{-3}$	2/14
		$(e^+ + e^-)/2$	0.155 ± 0.002	8.460 ± 0.030	0.652 ± 0.003	$(1.105 \pm 0.009) \times 10^{-2}$	8/24
	$1.4 < \lvert y\rvert < 2.0$	$(\mu^+ + \mu^-)/2$ (Open heavy decays)	0.125 ± 0.001	9.308 ± 0.022	0.799 ± 0.003	$(2.343 \pm 0.015) \times 10^{-2}$	7/9
	$1.2 < \lvert y\rvert < 2.2$	Drell – Yan $\rightarrow \mu^+\mu^-$	0.349 ± 0.002	8.849 ± 0.023	2.200 ± 0.004	$(1.559 \pm 0.001) \times 10^{-7}$	8/8
		$c\bar{c} \rightarrow \mu^+\mu^-$	0.385 ± 0.002	13.983 ± 0.023	1.509 ± 0.003	$(4.227 \pm 0.004) \times 10^{-9}$	10/11
		$b\bar{b} \rightarrow \mu^\pm\mu^\pm$	0.445 ± 0.002	20.501 ± 0.050	2.260 ± 0.030	$(6.917 \pm 0.006) \times 10^{-12}$	8/6
Figure 4(a) 2.76 TeV	$\lvert y\rvert < 0.9$	Inclusive γ	0.166 ± 0.001	6.791 ± 0.020	0.068 ± 0.002	$(3.565 \pm 0.035) \times 10^2$	32/14
	$2.5 < y < 4$	μ (From heavy decays)	0.345 ± 0.001	7.528 ± 0.021	0.000 ± 0.003	1.480 ± 0.002	7/12
	$\lvert y\rvert < 0.8$	e (From beauty decays)	0.315 ± 0.001	6.094 ± 0.016	1.000 ± 0.004	7.686 ± 0.051	3/16
		e (From heavy decays)	0.165 ± 0.001	4.305 ± 0.020	-0.043 ± 0.004	$(3.701 \pm 0.063) \times 10^2$	7/21
		$(e^+ + e^-)/2$ (Inclusive)	0.155 ± 0.002	5.554 ± 0.019	-0.05 ± 0.002	2.726 ± 0.057	7/15
Figure 6(a) 13 TeV	$\lvert\eta\rvert < 1.37$	$H \rightarrow$ diphoton	0.150 ± 0.001	14.681 ± 0.022	12.257 ± 0.004	$(5.295 \pm 0.186) \times 10^{-11}$	16/9
	$\lvert\eta\rvert < 0.8$	Heavy dielectron	0.125 ± 0.001	8.811 ± 0.019	2.281 ± 0.003	$(7.581 \pm 0.034) \times 10^{-1}$	6/13

Table 4: Values of T, n, a_0, σ_0, χ^2 and ndof corresponding to the dashed curves in Figures 2(a), 4(a), and 6(a) which are fitted by the convolution (Eq. (9)) of two TP-like functions. The participant quarks are listed together.

Figure	$y\,(\eta)$	Particle	Quark	T (GeV)	n	a_0	σ_0 (mb)	χ^2/ndof
Figure 2(a) 200 GeV	$\lvert\eta\rvert < 0.35$	Inclusive direct γ	$u\bar{u}$	0.383 ± 0.001	6.793 ± 0.024	0.060 ± 0.002	$(4.967 \pm 0.044) \times 10^{-3}$	2/14
		$(e^+ + e^-)/2$	$u\bar{u}$	0.236 ± 0.002	6.408 ± 0.020	-0.596 ± 0.003	$(1.192 \pm 0.008) \times 10^{-2}$	5/24
	$1.4 < \lvert y\rvert < 2.0$	$(\mu^+ + \mu^-)/2$ (Open heavy decays)	uc	0.167 ± 0.001	6.035 ± 0.025	-0.802 ± 0.003	$(2.226 \pm 0.014) \times 10^{-2}$	4/9
	$1.2 < \lvert y\rvert < 2.2$	Drell – Yan $\rightarrow \mu^+\mu^-$	$u\bar{u}$	0.418 ± 0.002	5.616 ± 0.023	0.398 ± 0.004	$(1.571 \pm 0.001) \times 10^{-7}$	8/8
		$c\bar{c} \rightarrow \mu^+\mu^-$	$c\bar{c}$	0.207 ± 0.002	4.072 ± 0.025	0.005 ± 0.004	$(4.206 \pm 0.004) \times 10^{-9}$	8/11
		$b\bar{b} \rightarrow \mu^\pm\mu^\pm$	$b\bar{b}$	0.207 ± 0.002	5.653 ± 0.024	0.049 ± 0.004	$(7.047 \pm 0.006) \times 10^{-12}$	3/6
Figure 4(a) 2.76 TeV	$\lvert y\rvert < 0.9$	Inclusive γ	$u\bar{u}$	0.233 ± 0.001	5.383 ± 0.019	-0.700 ± 0.003	$(3.345 \pm 0.020) \times 10^2$	27/14
	$2.5 < y < 4$	μ (From heavy decays)	$c\bar{c}$	0.309 ± 0.001	4.554 ± 0.022	-0.704 ± 0.003	1.364 ± 0.003	9/12
	$\lvert y\rvert < 0.8$	e (From beauty decays)	$b\bar{b}$	0.080 ± 0.001	1.993 ± 0.018	-0.150 ± 0.004	7.323 ± 0.042	4/16
		e (From heavy decays)	$c\bar{c}$	0.206 ± 0.002	2.441 ± 0.017	-0.894 ± 0.002	$(3.720 \pm 0.043) \times 10^2$	5/21
		$(e^+ + e^-)/2$ (Inclusive)	$u\bar{u}$	0.166 ± 0.001	3.724 ± 0.018	-0.700 ± 0.003	2.770 ± 0.021	12/15
Figure 6(a) 13 TeV	$\lvert\eta\rvert < 1.37$	$H \rightarrow$ diphoton	$c\bar{c}$	0.702 ± 0.001	4.573 ± 0.019	2.550 ± 0.003	$(5.376 \pm 0.209) \times 10^{-1}$	17/13
	$\lvert\eta\rvert < 0.8$	Heavy dielectron	$c\bar{c}$	0.166 ± 0.001	3.128 ± 0.021	-0.520 ± 0.002	$(7.581 \pm 0.034) \times 10^{-1}$	6/9

This means that the collision system gets further away from the equilibrium state at higher energy.

The values of revised index a_0, for the fits in Figures 1(a) and 3(a), listed in Table 1, show that maybe Eq. (7) is not useful because $a_0 \approx 1$. However, the values of a_0 listed in Table 3 show that Eq. (7) is indeed necessary because $a_0 \neq 1$. The values of a_0 for the fits in Figure 5(a) and listed in Table 1 are larger than 1 for nearly all heavy-flavor particles, while the values of a_0 for others are around 1. The values of a_0, for the fits in Figures 2(a), 4(a), and 6(a), listed in Tables 3

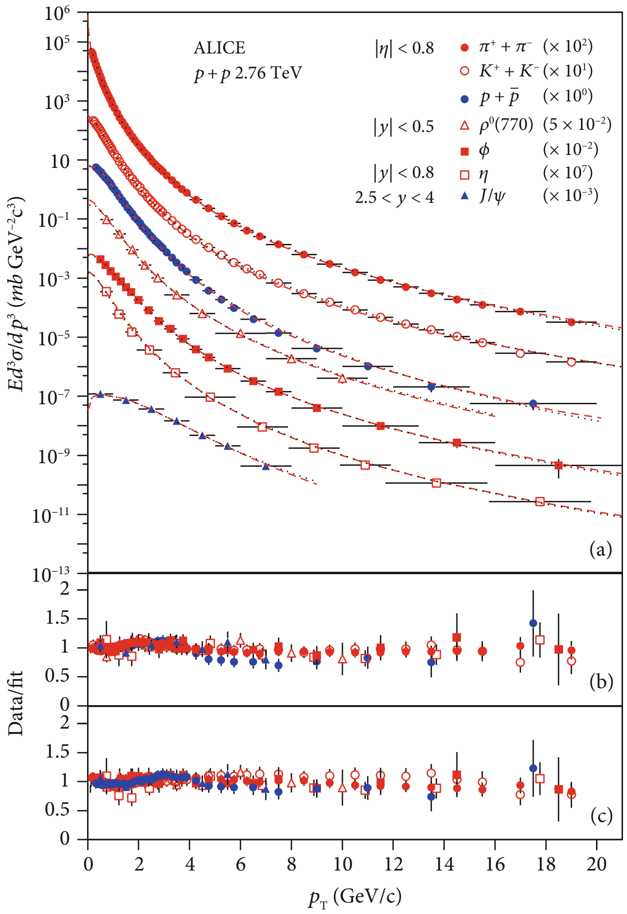

FIGURE 3: (a) The invariant cross-sections of different hadrons produced in $p + p$ collisions at 2.76 TeV. Different symbols represent different particles in different η or y ranges measured by the ALICE Collaboration [24–28] and scaled by different factors marked in the panel. The dotted and dashed curves are our fitted results by using Eqs. (7) and (9) or (11), respectively. (b) The ratio of data to fit obtained from Eq. (7). (c) The ratio of data to fit obtained from Eq. (9) or (11).

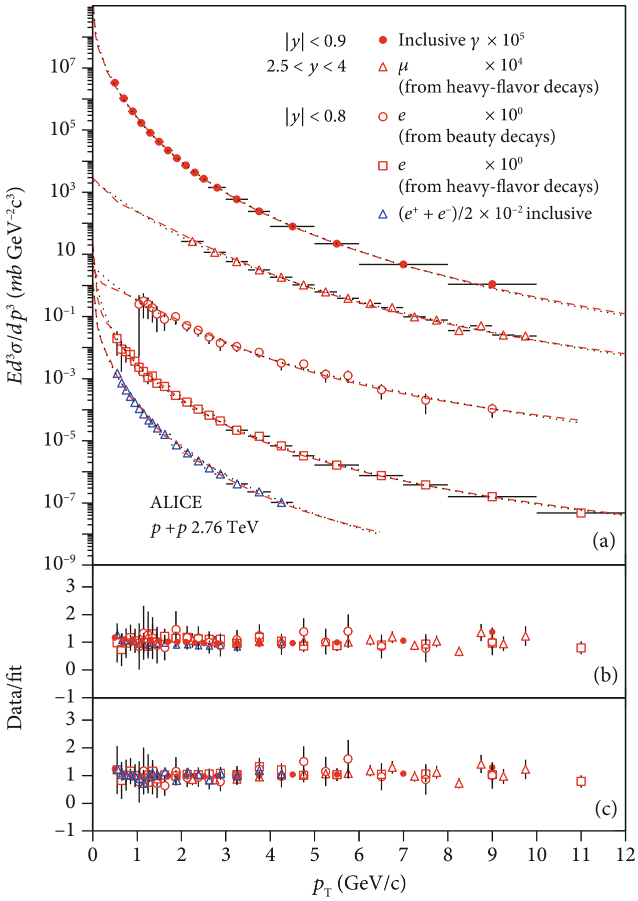

FIGURE 4: (a) The invariant cross-sections of photons and different leptons for a given combination of intermediate channel for $p + p$ collisions at 2.76 TeV. Different symbols represent different particles and their production channels in different y ranges measured by the ALICE Collaboration [29–32] and scaled by different factors marked in the panel. The dotted and dashed curves are our fitted results by using Eqs. (7) and (9), respectively. (b) The ratio of data to fit obtained from Eq. (7). (c) The ratio of data to fit obtained from Eq. (9).

and 4, are not equal to 1 in most cases. In general, Eq. (7) is necessary in the data-driven analysis because $a_0 \neq 1$ in most cases. In fact, Tables 1–4 show specific a_0 and corresponding collision energy, (pseudo) rapidity range, and particle type. Strictly, there are only two cases with $a_0 = 1$, that is the meson η production in pp collisions with $|\eta| < 0.35$ at 200 GeV (Table 1) and electron e from beauty decays in pp collisions with $|y| < 0.8$ at 2.76 TeV (Table 3).

To see the dependences of the spectra on free parameters, Figure 7 presents various pion spectra with different parameters in Eqs. (7) and (9). From the upper panel (Figures 7(a)–7(c)) to the middle panel (Figures 7(d)–7(f)) and then to the lower panel (Figures 7(g)–7(i)), T changes from 0.1 GeV to 0.15 GeV and then to 0.2 GeV. From the left panel to the middle panel and then to the right panel, n changes from 5 to 10 and then to 15. In each panel, the solid, dotted, dashed, and dot-dashed curves without (with) open circles correspond to the spectra with $a_0 = -0.1, 0, 1, \text{and } 2$, respectively, from Eq. (7) (Eq. (9)). One can see that the probability in the high p_T region increases with increasing T, decreases with increasing n, and increases with increasing a_0. From negative to positive, a_0 determines the shape in the low-p_T region.

From the shapes of curves in Figure 7, one can see that the parameter a_0 introduced in the TP-like function (Eq. (7)) by us determines mainly the trend of the curve in the low-p_T region. If the production of light particles via resonance decay affects obviously the shape of the spectrum, one may use a more negative a_0 in the fit. If the decay or absorbtion effect of heavy particles in the hot and dense medium in the participant region affects obviously the shape of the spectrum, one may use a more positive a_0 in the fit. Due to the introduction of a_0, the TP-like function is more flexible than the Tsallis–Pareto-type function. In fact, a_0 is a sensitive quantity to describe the influence of the production of light particles via resonance decay and the decay or

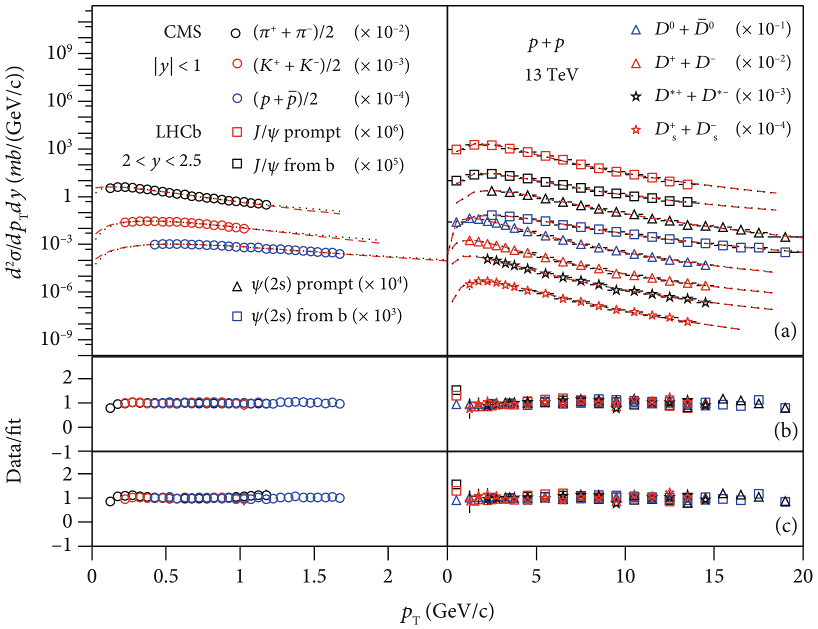

FIGURE 5: (a) The invariant cross-sections of different hadrons produced in $p+p$ collisions at 13 TeV. Different symbols represent different particles in different y ranges measured by the CMS [33] and LHCb [34–36] Collaborations and scaled by different factors marked in the panel. The dotted and dashed curves are our fitted results by using Eqs. (7) and (9) or (11), respectively. (b) The ratio of data to fit obtained from Eq. (7). (c) The ratio of data to fit obtained from Eq. (9) or (11).

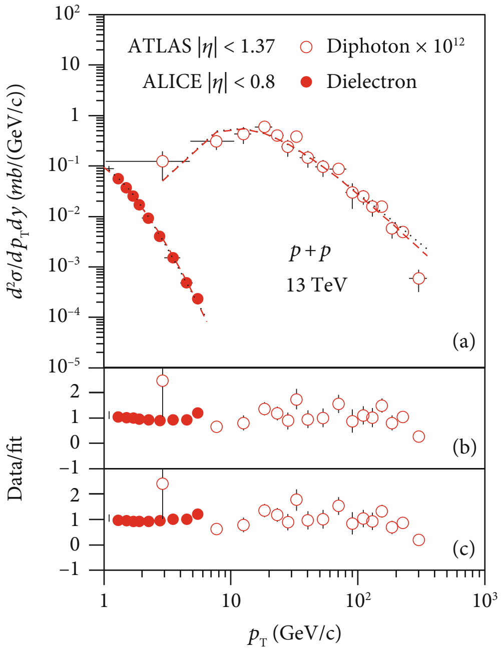

FIGURE 6: (a) The invariant cross-sections of $H \to$ diphotons and heavy-flavor dielectrons produced in $p+p$ collisions at 13 TeV. Different symbols represent different particles in different η ranges measured by the ATLAS [37] and ALICE [38] Collaborations and scaled by different factors marked in the panel. The dotted and dashed curves are our fitted results by using Eqs. (7) and (9), respectively. (b) The ratio of data to fit obtained from Eq. (7). (c) The ratio of data to fit obtained from Eq. (9).

absorbtion effect of heavy particles in hot and dense medium. Indeed, the introduction of a_0 is significant.

Before the summary and conclusions, we would like to point out that [9] proposes an alternative form of parametrization for the Tsallis-like function which also well describes the spectra in the low-p_T region, which we give as a major improvement of our fit. Indeed, although many theoretical or modelling works are proposed in high energy collisions, more works with different ideas are needed as the ways to systemize the experimental data in the field with fast progress.

4. Summary and Conclusions

We summarize here our main observations and conclusions.

(1) The transverse momentum spectra in terms of the (invariant) cross-section of various particles (different hadrons with given combinations and decay channels, photons, and different leptons with given combinations and production channels) produced in high energy proton-proton collisions have been studied by a TP-like function (a revised Tsallis–Pareto-type function). Meanwhile, the transverse momentum spectra have also been studied by a new description in the framework of the participant quark model or the multisource model at the quark level. In the model, the source itself is exactly the participant quark. Each participant quark contributes to the transverse momentum spectrum to be the TP-like function

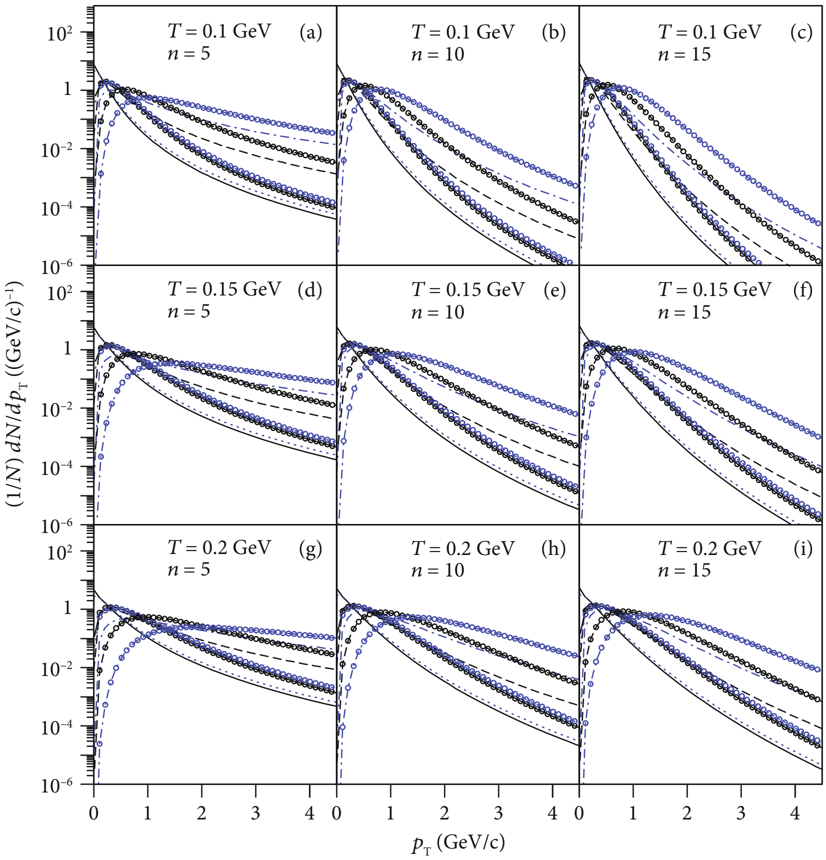

FIGURE 7: Various pion spectra with different parameters in Eqs. (7) and (9). From the upper panels ((a)–(c)) to the middle panels ((d)–(f)) and then to the lower panels ((g)–(i)), T changes from 0.1 GeV to 0.15 GeV and then to 0.2 GeV. From the left panels ((a), (d), (g)) to the middle panels ((b), (e), (h)) and then to the right panels ((c), (f), (i)), n changes from 5 to 10 and then to 15. In each panel, the solid, dotted, dashed, and dot-dashed curves without (with) open circles are obtained by $a_0 = -0.1,\ 0,\ 1,$ and 2, respectively, from Eq. (7) (Eq. (9)).

(2) For a hadron, the participant quarks are in fact constituent quarks. The transverse momentum spectrum of the hadron is the convolution of two or more TP-like functions. For a photon or lepton, the transverse momentum spectrum is the convolution of two TP-like functions due to two participant quarks, e.g., projectile and target quarks, taking part in the collisions. The TP-like function and the convolution of a few TP-like functions can fit the experimental data of various particles produced in proton-proton collisions at 200 GeV, 2.76 TeV, and 13 TeV measured by the PHENIX, ALICE, CMS, LHCb, and ATLAS Collaborations

(3) The values of effective temperature for the emissions of different hadrons do not depend on the collision energy, while for the emissions of photons and leptons, there is an obvious dependence on collision energy. This reflects the fact that the emission processes of photons and leptons are more complex than those of hadrons. In the central (pseudo) rapidity region, the effective temperature shows an increasing tendency with the increase of particle or quark mass. This reflects the fact that more collision energy is deposited to produce massive hadrons or to drive massive quarks to take part in the process of photon and lepton production

(4) The values of the power index are very large, which means that the values of the entropy index are very close to 1. The collision system considered in this study is approximately in an equilibrium state. The functions based on statistical methods are applicable in this study. In particular, with the increase of collision energy, the power index decreases and then the entropy index increases slightly. This means that the collision system gets further away from the equilibrium state at higher energy, though the entropy index is still close to 1 at the LHC

(5) The values of the revised index show that the TP-like function is indeed necessary due to the fact that this index is not equal to 1. In the TP-like function and its convolution, the effective temperature, power index, and revised index are sensitive to the spectra. In various pion spectra from the TP-like function and its convolution of two, the probability in the high transverse momentum region increases with the increase of effective temperature, decreases with the

increase of the power index, and increases with the increase of the revised index. From negative to positive, the revised index determines the shape in the low transverse momentum region, which is sensitive to the contribution of resonance decays

Data Availability

The data used to support the findings of this study are included within the article and are cited at relevant places within the text as references.

Ethical Approval

The authors declare that they are in compliance with ethical standards regarding the content of this paper.

Disclosure

The funding agencies have no role in the design of the study; in the collection, analysis, or interpretation of the data; in the writing of the manuscript; or in the decision to publish the results.

Conflicts of Interest

The authors declare that there are no conflicts of interest regarding the publication of this paper.

Acknowledgments

The first author (P.P.Y.) thanks Prof. Dr. David Blaschke and his colleagues of Bogoliubov Laboratory for Theoretical Physics of Joint Institute for Nuclear Research (Russia) for their hospitality, in where this work was partly performed. Her work was supported by the China Scholarship Council (Chinese Government Scholarship) under Grant No. 202008140170 and the Shanxi Provincial Innovative Foundation for Graduate Education under Grant No. 2019SY053. The work of the second author (F.H.L.) was supported by the National Natural Science Foundation of China under Grant Nos. 11575103 and 11947418, the Scientific and Technological Innovation Programs of Higher Education Institutions in Shanxi (STIP) under Grant No. 201802017, the Shanxi Provincial Natural Science Foundation under Grant No. 201901D111043, and the Fund for Shanxi "1331 Project" Key Subjects Construction. The work of the third author (R.S.) was supported by the financial supports from ALICE Project No. SR/MF/PS01/2014-IITI(G) of Department of Science & Technology, Government of India.

References

[1] M. Suleymanov, "The meaning behind observed p_T regions at the LHC energies," *International Journal of Modern Physics E*, vol. 27, no. 1, article 1850008, 2018.

[2] B. I. Abelev and STAR Collaboration, "Systematic measurements of identified particle spectra in *pp*, $d + Au$, and Au+Au collisions at the STAR detector," *Physical Review C*, vol. 79, article 034909, 2009.

[3] C. Y. Wong, G. Wilk, L. J. L. Cirto, and C. Tsallis, "From QCD-based hard-scattering to nonextensive statistical mechanical descriptions of transverse momentum spectra in high-energy pp and $p\bar{p}$ collisions," *Physical Review D*, vol. 91, article 114027, 2015.

[4] R. Hagedorn, "Multiplicities, p_T distributions and the expected hadron $\rightarrow$ quark $-$ gluon phase transition," *La Rivista del Nuovo Cimento*, vol. 6, no. 10, pp. 1–50, 1983.

[5] STAR Collaboration, "Strange particle production in $p + p$ collisions at $\sqrt{s} = 200$ GeV," *Physical Review C*, vol. 75, article 064901, 2007.

[6] C. Tsallis, "Possible generalization of Boltzmann-Gibbs statistics," *Journal of Statistical Physics*, vol. 52, no. 1-2, pp. 479–487, 1988.

[7] T. S. Biró, G. Purcsel, and K. Ürmössy, "Non-extensive approach to quark matter," *The European Physical Journal A*, vol. 40, no. 3, p. 325, 2009.

[8] H. Zheng, L. L. Zhu, and A. Bonasera, "Systematic analysis of hadron spectra in $p + p$ collisions using Tsallis distributions," *Physical Review D*, vol. 92, article 074009, 2015.

[9] H. Zheng and L. Zhu, "Can Tsallis distribution fit all the particle spectra produced at RHIC and LHC?," *Advances in High Energy Physics*, vol. 2015, Article ID 180491, 9 pages, 2015.

[10] D. Thakur, S. Tripathy, P. Garg, R. Sahoo, and J. Cleymans, "Indication of a differential freeze-out in proton-proton and heavy-ion collisions at RHIC and LHC energies," *Advances in High Energy Physics*, vol. 2016, Article ID 4149352, 13 pages, 2016.

[11] Z. B. Tang, Y. C. Xu, L. J. Ruan, G. van Buren, F. Q. Wang, and Z. B. Xu, "Spectra and radial flow in relativistic heavy ion collisions with Tsallis statistics in a blast-wave description," *Physical Review C*, vol. 79, no. article 051901, 2009.

[12] T. Mizoguchi, M. Biyajima, and N. Suzuki, "Analyses of whole transverse momentum distributions in $p\bar{p}$ and pp collisions by using a modified version of Hagedorn's formula," *International Journal of Moddern Physics A*, vol. 32, article 1750057, 2017.

[13] H.-L. Lao, F.-H. Liu, B.-C. Li, and M.-Y. Duan, "Kinetic freeze-out temperatures in central and peripheral collisions: which one is larger?," *Nuclear Science and Techniques*, vol. 29, no. 6, article 82, 2018.

[14] H.-L. Lao, F.-H. Liu, B.-C. Li, M.-Y. Duan, and R. A. Lacey, "Examining the model dependence of the determination of kinetic freeze-out temperature and transverse flow velocity in small collision system," *Nuclear Science and Techniques*, vol. 29, no. 11, article 164, 2018.

[15] CMS Collaboration, "Transverse-momentum and pseudorapidity distributions of charged hadrons in pp collisions at $\sqrt{s}$ $= 0.9$ and 2.36 TeV," *Journal of High Energy Physics*, vol. 2010, article 41, no. 2, 2010.

[16] CMS Collaboration, "Study of the inclusive production of charged pions, kaons, and protons in pp collisions at $\sqrt{s} =$ 0.9, 2.76, and 7 TeV," *The European Physical Journal C*, vol. 72, article 2164, 2012.

[17] CMS Collaboration, "Study of the production of charged pions, kaons, and protons in pPb collisions at $\sqrt{s_{NN}} = 5.02$ TeV," *The European Physical Journal C*, vol. 74, article 2847, 2014.

[18] CMS Collaboration, "Measurement of charged pion, kaon, and proton production in proton-proton collisions at $\sqrt{s} = 13$ TeV," *Physical Review D*, vol. 96, article 112003, 2017.

[19] PHENIX Collaboration, “Measurement of neutral mesons in $p+p$ collisions at $\sqrt{s}=200$ GeV and scaling production,” *Physical Review D*, vol. 83, article 052004, 2011.

[20] PHENIX Collaboration, “Heavy quark production in $p+p$ and energy loss and flow of heavy quarks in Au+Au collisions at $\sqrt{s_{NN}}=200$ GeV,” *Physical Review C*, vol. 84, article 044905, 2011.

[21] PHENIX Collaboration, “Direct photon production in p+p collisions at $\sqrt{s}=200$ GeV at midrapidity,” *Physical Review D*, vol. 86, article 072008, 2012.

[22] PHENIX Collaboration, “Measurements of $\mu\mu$ pairs from open heavy flavor and Drell-Yan in $p+p$ collisions at $\sqrt{s}=$ 200 GeV,” *Physical Review D*, vol. 99, article 072003, 2019.

[23] PHENIX Collaboration, “Cross section and transverse single-spin asymmetry of muons from open heavy-flavor decays in polarized $p+p$ collip sions at $\sqrt{s}=200$ GeV,” *Physical Review D*, vol. 95, article 112001, 2017.

[24] ALICE Collaboration, “Production of charged pions, kaons and protons at large transverse momenta in pp and Pb–Pb collisions at $\sqrt{s_{NN}}=2.76$ TeV,” *Physics Letters B*, vol. 736, pp. 196–207, 2014.

[25] ALICE Collaboration, “Production of the $\rho(770)^0$ meson in pp and Pb-Pb collisions at $\sqrt{s_{NN}}=2.76$ TeV,” *Physical Review C*, vol. 99, article 064901, 2019.

[26] ALICE Collaboration, “Production of π^0 and η mesons up to high transverse momentum in pp collisions at 2.76 TeV,” *The European Physical Journal C*, vol. 77, article 339, 2017.

[27] ALICE Collaboration, “$K^*(892)^0$ and $\phi(1020)$ meson production at high transverse momentum in pp and Pb-Pb collisions at $\sqrt{s_{NN}}=2.76$ TeV,” *Physical Review C*, vol. 95, article 064606, 2017.

[28] ALICE Collaboration, “Inclusive J/ψ production in *pp* collisions at $\sqrt{s}=2.76$ TeV,” *Physics Letters B*, vol. 718, pp. 295–306, 2012.

[29] ALICE Collaboration, “Direct photon production at low transverse momentum in proton-proton collisions at $\sqrt{s}=2.76$ and 8 TeV,” *Physical Review C*, vol. 99, article 024912, 2019.

[30] ALICE Collaboration, “Production of muons from heavy flavour decays at forward rapidity in pp and Pb-Pb collisions at $\sqrt{s_{NN}}=2.76$ TeV,” *Physical Review Letters*, vol. 109, article 112301, 2012.

[31] ALICE Collaboration, “Beauty production in pp collisions at $\sqrt{s}=2.76$ TeV measured via semi-electronic decays,” *Physics Letters B*, vol. 738, pp. 97–108, 2014.

[32] ALICE Collaboration, “Measurement of electrons from semileptonic heavy-flavor hadron decays in *pp* collisions at $\sqrt{s}=$ 2.76 TeV,” *Physical Review D*, vol. 91, article 012001, 2015.

[33] CMS Collaboration, “Measurement of charged pion, kaon, and proton production in proton-proton collisions at $\sqrt{s}=13$ TeV,” *Physical Review D*, vol. 96, article 112003, 2017.

[34] LHCb Collaboration, “Measurement of $\psi(2S)$ production cross-sections in proton-proton collisions at 7 and 13 TeV,” *The European Physical Journal C*, vol. 80, article 185, 2020.

[35] LHCb Collaboration, “Measurement of forward J/ψ production cross-sections in *pp* collisions at $\sqrt{s}=13$ TeV,” *Journal of High Energy Physics*, vol. 2015, no. 10, article 172, 2015.

[36] LHCb Collaboration, “Measurements of prompt charm production cross-sections in *pp* collisions at $\sqrt{s}=13$ TeV,” *Journal of High Energy Physics*, vol. 2016, no. 3, article 159, 2016.

[37] The ATLAS Collaboration, “Measurements and interpretations of Higgs-boson fiducial cross sections in the diphoton decay channel using fb^{-1} of *pp* collision data at $\sqrt{s}=13$ TeV with the ATLAS detector,” in *ATLAS-CONF-2019-029, European Physical Society Conference on High Energy Physics (EPS-HEP) 2019*, Ghent, Belgium, 2019.

[38] ALICE Collaboration, “Dieletron and heavy-quark production in inelastic and high multiplicity proton–proton collisions at $\sqrt{s_{NN}}=13$ TeV,” *Physics Letters B*, vol. 788, pp. 505–518, 2019.

[39] ALICE Collaboration, “Measurement of inelastic, single- and double-diffraction cross sections in proton–proton collisions at the LHC with ALICE,” *The European Physical Journal C*, vol. 73, article 238, 2013.

[40] K.-C. Chou, L.-S. Liu, and T.-C. Meng, “Koba-Nielsen-Olesen scaling and production mechanism in high energy collisions,” *Physical Review D*, vol. 28, pp. 1080–1085, 1983.

[41] G.-R. Zhou, *Probability Theory and Mathematical Statistics*, Higher Education Press, Beijing, China, 1984.

[42] P.-P. Yang, Q. Wang, and F.-H. Liu, “Mutual derivation between arbitrary distribution forms of momenta and momentum components,” *International Journal of Theoretical Physics*, vol. 58, no. 8, pp. 2603–2618, 2019.

[43] L.-L. Li and F.-H. Liu, “Excitation functions of Tsallis-like parameters in high-energy nucleus-nucleus collisions,” 2020, https://arxiv.org/abs/2006.15333.

[44] E. K. G. Sarkisyan, A. N. Mishra, R. Sahoo, and A. S. Sakharov, “Multihadron production dynamics exploring the energy balance in hadronic and nuclear collisions,” *Physical Review D*, vol. 93, no. article 054046, 2016.

[45] E. K. G. Sarkisyan and A. S. Sakharov, “Relating multihadron production in hadronic and nuclear collisions,” *The European Physical Journal C*, vol. 70, no. 3, pp. 533–541, 2010.

[46] E. K. G. Sarkisyan and A. S. Sakharov, “Multihadron production features in different reactions,” *AIP Conference Proceedings*, vol. 828, pp. 35–41, 2006.

[47] E. K. Sarkisyan-Grinbaum, A. Nath Mishra, R. Sahoo, and A. S. Sakharov, “Effective-energy universality approach describing total multiplicity centrality dependence in heavy-ion collisions,” *EPL*, vol. 127, no. article 62001, 2019.

[48] A. N. Mishra, A. Ortiz, and G. Paić, “Intriguing similarities of high-p_T particle production between *pp* and *A-A* collisions,” *Physical Review C*, vol. 99, article 034911, 2019.

[49] P. Castorina, A. Iorio, D. Lanteri, H. Satz, and M. Spousta, “Universality in hadronic and nuclear collisions at high energy,” *Physical Review C*, vol. 101, no. article 054902, 2020.

[50] E. K. G. Sarkisyan, A. N. Mishra, R. Sahoo, and A. S. Sakharov, “Centrality dependence of midrapidity density from GeV to TeV heavy-ion collisions in the effective-energy universality picture of hadroproduction,” *Physical Review D*, vol. 94, article 011501(R), 2016.

[51] A. N. Mishra, R. Sahoo, E. K. G. Sarkisyan, and A. S. Sakharov, “Effective-energy budget in multiparticle production in nuclear collisions,” *The European Physical Journal C*, vol. 74, no. 11, p. 3147, 2014.

[52] F.-H. Liu, “Unified description of multiplicity distributions of final-state particles produced in collisions at high energies,” *Nuclear Physics A*, vol. 810, no. 1-4, pp. 159–172, 2008.

[53] F.-H. Liu, Y.-Q. Gao, T. Tian, and B.-C. Li, “Unified description of transverse momentum spectrums contributed by soft and hard processes in high-energy nuclear collisions,” *The European Physical Journal A*, vol. 50, no. 6, article 94, 2014.

[54] Z.-J. Xiao and C.-D. Lü, *Introduction to Particle Physics*, Science Press, Beijing, China, 2016.

[55] T. Feldmann, P. Kroll, and B. Stech, “Mixing and decay constants of pseudoscalar mesons,” *Physical Review D*, vol. 58, no. - article 114006, 1998.